

FEATURE ARTICLE

[View Article Online](#)
[View Journal](#) | [View Issue](#)


Cite this: *Chem. Commun.*, 2015,
 51, 10261

Some recent developments in surface and interface design for photocatalytic and electrocatalytic hybrid structures

Song Bai and Yujie Xiong*

The surface and interface are considered as the crucial features that can be engineered to improve the performance of catalysts. The great advancements in both controlled syntheses and catalytic mechanism studies have paved the way for the rational surface and interface design of catalysts. In this feature article, we overview our recent progress in surface and interface design for well-defined hybrid structures mainly toward the photocatalytic and electrocatalytic applications in which charge carriers play an important role. First, we outline the surface parameters of components including exposed facets, compositions, surface areas and crystal phases that have been tailored toward higher surface activation abilities for electrocatalytic and photocatalytic reactions. Second, we summarize the designing rules for the interface between two components to favor the charge transfer for photocatalytic reactions on the surface. Furthermore, we outline the synergistic effects on photocatalysis and electrocatalysis through the simultaneous control of the surface and the interface, which can also be extended to enhance other catalytic reactions (e.g., CO oxidation). Finally, we discuss the challenges and opportunities for further development of surface and interface design toward catalytic performance tuning.

Received 1st April 2015,
 Accepted 15th May 2015

DOI: 10.1039/c5cc02704g

www.rsc.org/chemcomm

Hefei National Laboratory for Physical Sciences at the Microscale, iChEM (Collaborative Innovation Center of Chemistry for Energy Materials), and School of Chemistry and Materials Science, University of Science and Technology of China, Hefei, Anhui 230026, P. R. China. E-mail: yixiong@ustc.edu.cn;
 Fax: +86 551-63606657



Song Bai received his BS and MS degrees from Jiangsu University in 2009 and 2012, respectively. He is currently a PhD candidate under the tutelage of Professor Yujie Xiong at the University of Science and Technology of China. His research interest focus on design and synthesis of novel hybrid nanomaterials for photocatalysis.

Song Bai

Introduction

Design and production of catalytic materials with high activity, selectivity and stability for a determined catalytic reaction are always the ultimate goal of catalyst manufacturers.^{1,2} To achieve this goal, the size, geometry, composition, phase and



Yujie Xiong

Yujie Xiong received his BS in chemical physics in 2000 and PhD in inorganic chemistry in 2004 (with Professor Yi Xie), both from the University of Science and Technology of China (USTC). After four-year training with Professors Younan Xia and John A. Rogers, he joined NSF-NNIN at Washington University in St. Louis as the Principal Scientist and Lab Manager. From 2011, he has been a Professor of Chemistry at the USTC. He has published 101 papers with over 8000 citations (H-index 47). His research interest includes synthesis, fabrication and assembly of inorganic materials for energy and environmental applications.

architecture structure of the catalytic materials have been tailored and optimized with great efforts and by different methodologies.^{3–5} Nowadays, micro/nanomaterials have been widely used as catalysts in various catalytic reactions, which show potential applications for renewable energy production and environmental remediation.^{6,7} Among various systems, photocatalysis and electrocatalysis are two classes of reactions in which charge carriers play an important role.

On the route to the improved catalytic properties in these reactions, two development trends have emerged for the micro/nanocatalysts. One is that catalysts have been developed from single-component homogeneous structures to multi-component hybrid structures.^{8,9} The major motivation is that the integration by different components opens the possibilities for making up the shortage of each component and forming a synergistic effect for enhanced catalytic performance. In the hybrid structures, some specific components can provide active sites for surface reactions with high molecular activation ability, while the other components play roles in supporting the operation of surface catalysis, such as charge production in photocatalysis as well as charge transfer in both photocatalysis and electrocatalysis. For instance, many review articles on the topic of graphene-based hybrid catalysts have been published for enhanced photocatalytic or electrocatalytic performance in recent years.^{10–12}

The other trend is that the design of the surface and the interface of materials is of increasing importance for optimizing the performance of photocatalytic and electrocatalytic materials. It is well known that the catalytic reactions occur mainly on the surface of catalysts, which is generally applicable to heterogeneous catalysis. In other words, most of the catalytic active sites should be located on the catalyst surface. For this reason, the surface conditions, including surface compositions, structures, areas, pores, and vacancies, greatly impact the activity and selectivity of the catalyst as these parameters determine the surface adsorption and activation abilities of particular reactants.^{13,14} When the design of catalytic materials involves multiple components, the interface between two components in hybrid structures stands out as another important parameter. On one hand, the interface is the location where charge carriers are transferred between the components for surface catalytic reactions, and as such, their transfer efficiency heavily depends on the interfacial structures.¹⁵ For instance, it is known that interfacial defects are often the centers for electron–hole recombination, thus impeding the charge transfer in photocatalysis.^{16,17} On the other hand, some additional interfacial effects such as the surface polarization effect may play important roles in tuning the molecular activation ability of the catalyst surface.¹⁸ In general, tailoring the surface and the interface of hybrid structures would be a promising direction for photocatalyst and electrocatalyst development in the future.

To date, catalytic mechanism research has guided us to design the surface and the interface of high-performance photocatalysts and electrocatalysts toward our demand,¹⁹ while advanced synthetic approaches can help to put the designs into reality.^{20,21} As a two-way research mode, the new structures obtained through surface/interface design and controlled syntheses offer a set of clear and well-defined platforms for

further understanding the working mechanisms that remained unexplored in the past.^{18,22–28} This two-way research mode has been widely used for catalyst design and catalytic mechanism research. In this Feature Article, we summarize the recent research efforts by our research group along this research mode, demonstrating how to tailor the surface and the interface in hybrid structures for enhanced performance in photocatalysis and electrocatalysis. We first outline the surface parameters of the components in hybrid structures that can be tuned to enhance the catalytic activity and selectivity. The surface with tightly controlled exposed facets, compositions, areas and phases has shown important contributions to both electrocatalytic and photocatalytic reactions. Then we discuss the interface between two components that has been optimized to facilitate the charge transfer for surface photocatalytic reactions. In the last part of this article, we highlight our most recent studies that integrate the surface and interface designs for further catalytic performance enhancement through their synergistic interactions such as the surface polarization effect, which can be extended from photocatalysis and electrocatalysis to other reaction types such as CO oxidation.

For a bare homogeneous catalyst, the material is only covered by a continuous surface without any interface formed between solid matters. As the models switch to hybrid structures, two or more components are involved to make the situation more complicated due to different combination configurations of the components, formulating various types of surfaces and interfaces. In the literature,¹⁵ three classic configuration models are basically present in terms of the relative locations of two components in a catalytic hybrid structure: supported structure, heterostructure, and core–shell structure (Fig. 1). Other configurations can be assigned to the derivation of one model or the combination of multiple models. There is no doubt that the configuration models have their own advantages and disadvantages with regard to the surface and the interface. Thus choosing an appropriate configuration model for a specific reaction system is the first step in the surface and interface design for hybrid structures. From the viewpoint of sample preparation, the growth models and the difficulty in their syntheses also depend on the configurations and material types, in which many factors for the components including lattice mismatch, hydrophilicity or hydrophobicity, bonding and dissociation energies may make the difference.

In the supported structure, a certain amount of component I at smaller sizes is loaded on component II with larger particle sizes.^{28,29} In a single supported structure, one continuous surface of component II appears in the system, while the populations of the discrete surface of component I and the interface between components I and II are determined by the number of component I particles. In the synthesis, the structure is often obtained through non-epitaxial growth with multiple nucleation sites or a self-assembly method, which simplifies their synthesis without the need of bothering the consideration of interfacial energy and lattice mismatch between the components. The straightforward synthetic scheme also facilitates the control of the surface and the interface in this structure. However, the non-epitaxial growth or

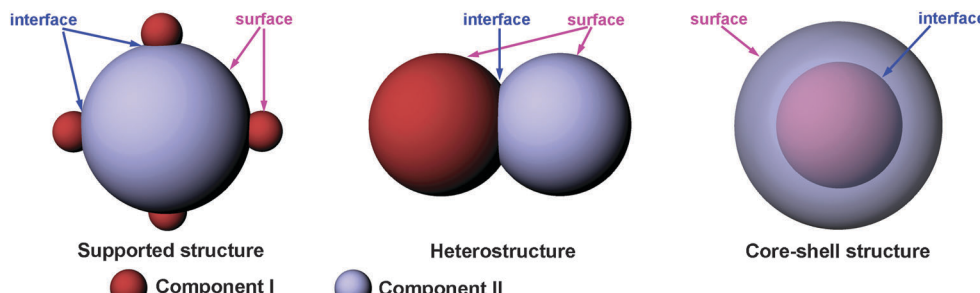


Fig. 1 Schematic illustration for the interface and the surface in basic catalytic hybrid architectural structures.

the self-assembly method may also lead to a large number of defects at the interface, which blocks the interfacial charge transfer and initiates the interfacial corrosion.

The heterostructure (*i.e.*, Janus structure) resembles the supported configuration, but comprises only one particle for each component in a single structure whose particle size is usually comparable to each other.^{30,31} For this reason, each component is bound by one continuous surface, and an interface is formed between the two components. This structure is often fabricated through non-epitaxial or epitaxial growth with one component being incompletely wetted by the other. Compared with the supported structure, intuitively it should be more difficult to synthesize this structure on a large scale and in high quality as the nucleation and further growth of one component have to be controlled in specific sites on the other one. The structure obtained through epitaxial growth often has low interfacial defects. However, in order to achieve this growth mode, small lattice mismatches or similar compositions between the two components are often required to reduce the interfacial energy and initiate the nucleation.^{31,32}

The core–shell structure is formed by coating the component I core with the component II shell.^{33,34} Unlike the supported structure and heterostructure, only the surface of component II in this structure is exposed to reaction medium, making it suitable for the reaction that takes place only on component II. The interface between the components is fully protected by the shell, thus staying away from corrosion. Similar to the heterostructure, the structure is synthesized through either non-epitaxial or epitaxial growth models except that component I is completely wetted by component II. For the two components with small lattice mismatches, a low interfacial energy may favor the epitaxial growth. However, the epitaxial growth limits surface and interface engineering, as the interfacial structure totally depends on the lattice of the core – the same as the surface structure of the shell.³⁵ As for the two components with large lattice mismatches, surface modification of the core is often needed to lower the interfacial energy for shell coating, which may lead to a large number of interfacial defects.³⁶

Surface design for electrocatalytic and photocatalytic hybrid structures

The above section informs us of the different mechanisms for surface and interface formations in various hybrid structures as

well as their merits and limitations. Based on the analyses, we can choose one appropriate configuration and corresponding components for specific catalytic reactions, and further carry out surface and interface design. In this section, we are in the position to outline our studies on the surface design for the components in the catalytic hybrid structures.

Prior to the discussions on specific cases of surface design, some designing rules which we have been followed in the design should be clarified. Firstly, the surface to be designed should be the location where the activation reactions take place. Not all the surface in hybrid structures can participate in the reactions, and as a result, the parameter tuning of the catalytically inactive surface does not enhance catalytic performance. For instance, component II in some supported structures only plays the role as a support without catalytic sites on the surface, which mainly prevents the aggregation of component I in catalytic reactions.³⁷ Secondly, surface catalytic mechanisms provide important insights for us to rationally tune key parameters, as the surface parameters determining catalytic performance might be quite different for various types of reactions. A typical example is that the pore sizes of porous components can be tuned to increase reaction selectivity according to the molecular sizes of reactants or products. By selecting appropriate pore sizes, large-sized reactants can be prevented from entering pores/channels and undergoing reactions, and at the same time, large-sized products are blocked to leave the surface. This surface design approach is only applicable to the shape-selective catalytic reactions involving different molecular sizes of reactants, products or intermediates.³⁸ Thirdly, the correlation of surface parameters with interface structures has to be considered, especially in the case that interfacial behavior affects catalytic performance on the surface. For example, surface vacancies may facilitate catalytic reactions since dangling bonds in the vacancies are prone to accept charge carriers and reactants.³⁹ However, when an interface is formed based on the surface with vacancies, the vacancies would become the interfacial defects that are harmful to charge transfer in the reactions.⁴⁰

According to these rules, we have performed surface designs for both electrocatalytic and photocatalytic hybrid structures. Here we first outline our progress in electrocatalysis. Given the difficulty of surface design in hybrid structures – such a complex system with multiple components, we initiate surface catalytic research using single-component catalysts in certain

cases. A typical case is the design of hybrid structures which have branched Pt nanocrystals supported on graphene nanosheets for electrocatalysis in oxygen reduction reaction (ORR).²⁹ To design Pt surface structure toward high electrocatalytic activities, this study starts with the performance comparison of Pt nanocrystals with different numbers of branches.^{22,41} It turns out that octopods exhibit superior catalytic performance to their counterparts (*i.e.*, hexapods, tetrapods and tripods), mainly attributed to the high densities of stepped surface atoms on {311} high-index exposed facets (Fig. 2a). The active surface areas have been tuned from 0.39 to 1.32 cm² by increasing the numbers of branches.⁴¹ Based on this finding, we further assemble Pt highly concave cubes (HCCs) whose surface structures are analogous to the octopods with reduced graphene oxide (rGO) for ORR reaction (Fig. 2b and c).²⁹ Both the catalytic activity and stability of the Pt HCCs have been greatly enhanced by their integration with rGO. rGO not only improves the conductivity of catalysts on electrodes and promotes the catalyst-electrode adhesion to facilitate their charge transfer, but also suppresses the agglomeration and oxidation erosion of Pt catalysts (Fig. 2d and e).^{42,43}

The design approach to Pt HCC-rGO hybrid structures is a straightforward method in which rGO only serves as a support for performance enhancement and does not participate in the formation of catalytic components (*i.e.*, Pt in this case). Thus the design of this hybrid structure is mainly based on the early screening of surface parameters for the catalytic component. The case of PtPd nanocage-rGO structures follows a very different approach to the surface design, as rGO plays an important role in the formation of Pt nanocages.⁴⁴ In the synthesis, this unique hybrid structure is created through a three-step process using Pd nanocubes as templates (Fig. 3a): (1) *in situ* growth of Pd nanocubes (11–12 nm) on rGO (Fig. 3b);

(2) selective coating of Pt shells (~ 1.5 nm in thickness) on the Pd surface through an epitaxial growth process to form Pt-Pd-rGO structures (Fig. 3c); and (3) removal of the Pd nanocubes through chemical etching to produce PtPd nanocage-rGO structures (with trace amounts of residual Pd, Fig. 3d). In this work, the surface parameters of hybrid structures are designed step by step toward catalytic performance enhancement, including the transformation of the Pd{100} to Pt{100} surface with higher ORR activity⁴⁵ by coating Pt shells and the evolution of solids to hollow structures to double surface area through removing Pd cores. The increased surface area together with the highly active Pt surface boosts the ORR activity. As shown in Fig. 3e and f, the catalytic activity increases in the order: Pd nanocube-rGO < Pt nanocube-rGO < Pt-Pd-rGO < PtPd nanocage-rGO. In this assessment, Pd and rGO loadings are kept the same for Pd nanocube-rGO and Pt-Pd-rGO, while Pt and rGO loadings are consistent for Pt nanocube-rGO, Pt-Pd-rGO and PtPd nanocage-rGO. The active surface areas of Pt nanocube-rGO, Pt-Pd-rGO and PtPd nanocage-rGO have been determined to be 8.78, 9.50 and 11.10 cm², respectively. This research demonstrates that surface textual factors including the surface composition and area are important parameters for ORR reactions. Certainly, similar to the case of Pt HCC-rGO, the positive role of rGO cannot be neglected here.

In addition to electrocatalysis, surface design also holds the promise for the optimization of hybrid structures for

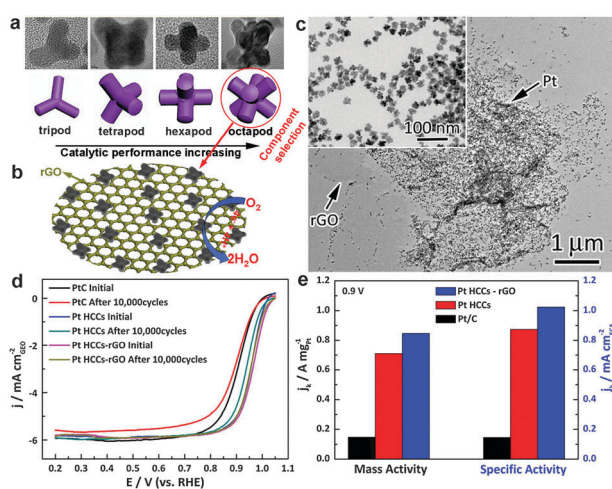


Fig. 2 (a) Schematic illustration showing the tunable electrocatalytic performance of Pt multipods (adapted with permission from ref. 41, Copyright 2012 American Chemical Society). (b and c) Schematic illustration and TEM images of the Pt HCC-rGO hybrid structure; (d) ORR polarization curves of Pt HCCs and Pt HCC-rGO samples with Pt/C before and after 10 000 cycles; (e) mass activity and specific activity at 0.9 V versus RHE (adapted with permission from ref. 29, Copyright 2013 Nature Publishing Group).

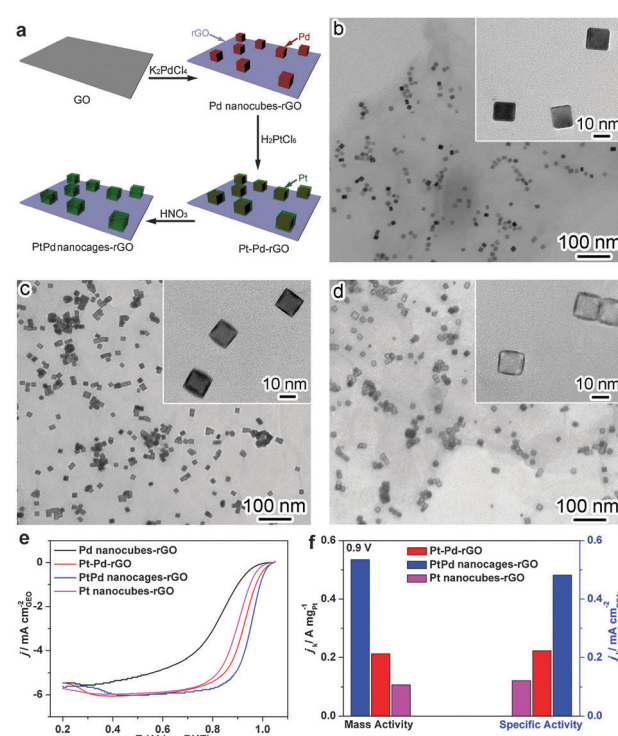


Fig. 3 (a) Schematic illustration for the synthesis of PtPd nanocage-rGO hybrid structure; (b-d) TEM images of (b) Pd nanocube-rGO, (c) Pd-Pt-rGO, and (d) PtPd nanocage-rGO hybrid structures; (e) ORR polarization curves of as-obtained catalysts; (f) mass activity and specific activity of Pt-based catalysts at 0.9 V versus RHE (adapted with permission from ref. 44, Copyright 2015 Springer).

photocatalysis. For the single-component photocatalyst based on a bare semiconductor, the impacts of surface parameters such as facets, compositions and vacancies on catalytic performance have been widely investigated.^{46,47} However, the alteration of these parameters may also lead to the variation in the light absorption ability of semiconductors for charge generation,^{48,49} formulating an obstacle to clarify the contributions of parameter adjustment to catalytic performance. In contrast, co-catalysts in hybrid structures offer us an alternative surface design route, which mainly traps electrons or holes from the light-harvesting semiconductor as well as serves as the active sites for reduction or oxidation reactions.⁵⁰ As the co-catalysts are not involved in light absorption, it becomes more straightforward to tune the catalytic performance by tailoring the surface parameters of co-catalysts so that the factor of light absorption can be excluded.

A typical case in our research is the decoration of Pd nanocrystals on g-C₃N₄ nanosheets to form hybrid structures, in which Pd exposed with different facets is used as a co-catalyst.⁵¹ Using different capping agents, Pd nanocubes enclosed with {100} facets and Pd nanotetrahedrons with {111} facets can be selectively *in situ* grown on C₃N₄ nanosheets, respectively (Fig. 4a–c). In both hybrid structures, the electrons photo-generated on C₃N₄ are transferred to the Pd surface with equivalent efficiency for the reduction of H₂O and CO₂. As a result, C₃N₄-Pd nanotetrahedrons prefer reducing CO₂ with H₂O to carbon products. In comparison, C₃N₄-Pd nanocubes mainly undergo H₂O reduction to produce H₂. Given the comparable charge generation and transfer in both cases, we have been able to reliably assess that Pd{111} facets offer higher CO₂ adsorption energy and lower CO₂ activation barriers while Pd{100} facets show much higher H₂O adsorption energy.

In addition to the facet, the surface phase of co-catalyst is also an important parameter to surface design, as illustrated by one of our recent studies that MoS₂ nanosheets are employed as co-catalysts for H₂ evolution.⁵² By implementing an assembly and *in situ* growth method, the same TiO₂ semiconductor nanocrystals can be loaded on MoS₂ nanosheets in the octahedral (1T) phase and the trigonal prismatic (2H) phase, respectively (Fig. 4d and e). In 2H MoS₂, the active sites for H₂ production are only located at the edges of nanosheets,⁵³ and this semiconducting phase can only offer relatively low mobility for charge transport.⁵⁴ In comparison, the metallic 1T MoS₂ nanosheets have additional reaction sites on their basal plane,⁵⁵ and possess higher charge transport mobility. Thus the higher diffusion rate and the shorter diffusion distance enabled by the 1T phase would allow significantly more TiO₂-generated electrons to arrive at the reaction sites and participate in the H₂ evolution reactions before they lose their lives (Fig. 4f). As such, the obtained TiO₂-MoS₂(1T) structure has shown a dramatically higher photocatalytic H₂ production rate in comparison with that of TiO₂-MoS₂(2H) structure (Fig. 4g). In general, the fundamental goal of surface design for hybrid structures is to create the maximum number of reaction sites with high activities on the surface for the given reactions, so as to optimize catalytic activity and selectivity.

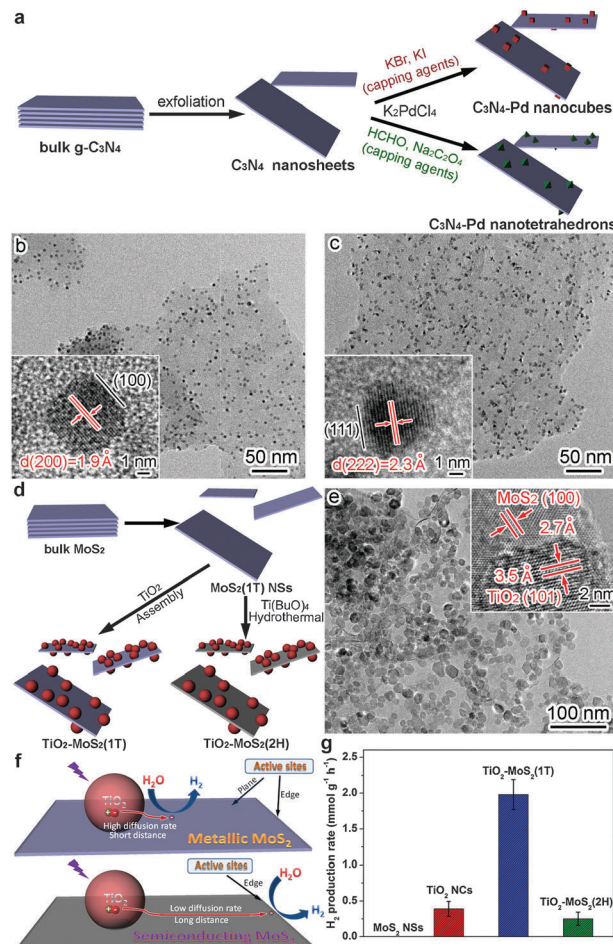


Fig. 4 (a) Schematic illustration for the synthesis of C₃N₄-Pd hybrid structures; (b and c) TEM and HRTEM (inset) images of (b) C₃N₄-Pd nanocubes and (c) C₃N₄-Pd nanotetrahedrons (adapted with permission from ref. 51, Copyright 2014 Royal Society of Chemistry). (d) Schematic illustration for the synthesis of TiO₂-MoS₂ hybrid structures; (e) TEM and HRTEM (inset) images of TiO₂-MoS₂(1T) hybrid structure; (f) schematic illustrating charge-transfer behavior and H₂ evolution active sites for TiO₂-MoS₂(1T) and TiO₂-MoS₂(2H); (g) photocatalytic average rates of H₂ production under UV light irradiation (adapted with permission from ref. 52, Copyright 2015 Springer).

Interface design for photocatalytic hybrid structures

While surface design is regarded as materials engineering that controls the interactions of reaction species with the exterior material of a component, interface design represents an aspect for harnessing catalytic behavior by engineering the interior structures embedded between two components. Undoubtedly, the interface design is also a challenging task. The surface design can be still performed using a post-synthesis process like the example of surface composition transformation from Pd{100} in Pd nanocube-rGO to Pt{100} in Pt-Pd-rGO as discussed above.⁴⁴ Differently it would be extremely difficult to modify the interface embedded between the components as long as the hybrid structure is formed. As the interface is mainly inherited from the surface structure of a pre-synthesized

component, any nonuniform surface would lead to a low-quality interface in a hybrid structure. Thus an ideal interface design requires the components to have well-designed and defined surface structures prior to the synthesis of hybrid structures.

To achieve a successful interface design, some specific designing rules were kept in our mind. First of all, the interface should be designed to maneuver the catalytic performance of a component in hybrid structures. In this sense, the design of an interface where charge carriers cannot be efficiently transferred between two components toward surface reactions must be a failure.⁵⁶ Secondly, similar to surface design, there are many interface parameters to be tailored, including interfacial area, compositions, defects, facets and electronic coupling, and the distance from the interface to the surface. Accordingly adjustments should be made on certain interface parameters depending on the configurations of hybrid structures and types of reactions. For instance, interfacial defects often appear as the centers where charge trapping or scattering occurs, detrimental to the participation of charges in surface catalytic reactions;⁴⁰ however, in a all-solid-state Z-scheme photocatalyst with direct contact of two semiconductors, interfacial defects are indispensable for its operation.⁵⁷ Thirdly, without external voltage, the charge transfer direction across the interface, with a dependence on the work functions of two components, should be analyzed and made consistent with the requirements for surface reactions.⁵⁸ In general, when an interface is designed to transfer electrons for the surface reactions, the work function of the component for accepting the electrons should be higher than that of the other component. The last factor that should be taken into account in the sample comparison is that altering interface parameters may also cause the changes in surface parameters.

In our research, the interface design has been mainly performed to steer charge transfer for photocatalytic reactions. For bare semiconductor catalysts, the migrations of photo-generated electrons and holes take place randomly, resulting in the high probability of charge recombination and low photocatalytic efficiency. When an interface is formed between two components with different work functions, an internal electric field will be established to drive electrons or holes to transfer from one component to the other across the interface. As such, electrons and holes can be spatially separated toward different components to reduce charge recombination.^{19,59} This process makes the electrons and holes accumulate on the surfaces of two components to enable high reactive abilities for reduction and oxidation, respectively. Therefore, the interface is the function location for charge separation and transfer, which greatly determines the performance of photocatalytic hybrid structures. Thus the interface should be designed to offer a driving force for the unidirectional electron or hole transfer and in turn realize the charge spatial separation. Certainly the interface parameters should be optimized for high-efficiency charge transfer for surface reactions.

As briefly mentioned above, the work functions of interfacing components should be considered for the unidirectional

charge transfer across the interface, whose importance has been clearly demonstrated by Pd–Cu₂O supported structures with various Cu₂O–Pd interfaces.²⁸ This work shows that various surface facets may have different work functions, and this difference drives photogenerated electrons and holes to reach different crystal facets, respectively.⁶⁰ In the case of Cu₂O cuboctahedrons, the work function of Cu₂O{100} (*ca.* 7.2 eV) is much higher than that of Cu₂O{111} (*ca.* 4.8 eV), accumulating electrons and holes on the {100} and {111} surface, respectively (Fig. 5a). To facilitate charge separation, a Schottky junction can be built between p-type semiconductor Cu₂O and metal Pd to trap the photogenerated holes. Although the spatial charge separation of Cu₂O designates {111} facets as the locations for hole accumulation, the Schottky junction cannot be formed at the Cu₂O{111}–Pd interface as Cu₂O{111} has a lower work function than Pd, which makes the hybrid structures with Pd being selectively deposited on the {111} surface (Fig. 5b) not work for hole trapping. In stark contrast, the Cu₂O{100}–Pd interface favors the migration of holes simply because of the higher work function of Cu₂O{100} in favor of the Schottky barrier establishment. For this reason, only the Pd–Cu₂O supported structure having the Cu₂O{100}–Pd interface can be used as an alternative hybrid structure for hole trapping (Fig. 5c). As shown in Fig. 5d, the Pd–Cu₂O{100} supported structure shows much more prominent H₂ production in comparison with other Cu₂O counterparts, whose efficiencies depend on the densities of decorated Pd nanoparticles.

Besides the selection of appropriate facets in interface formation for charge transfer, the interface structure between the selected components is another important factor. A typical case is the comparison of charge transfer abilities of the Cu₂O–Pd

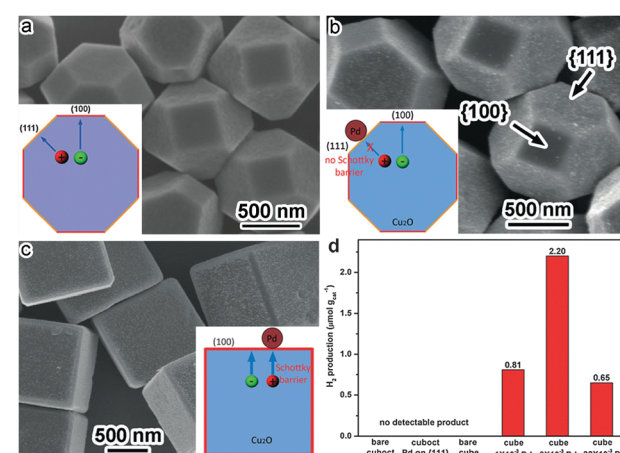


Fig. 5 (a) SEM image of Cu₂O cuboctahedrons and illustration for the charge spatial distribution between the Cu₂O{100} and Cu₂O{111} surface; (b) SEM image of Cu₂O cuboctahedrons whose {111} surface is selectively decorated with Pd and illustration for the charge transfer on the Cu₂O{111}–Pd interface; (c) SEM image of Cu₂O cubes with {100} facets that are decorated with Pd (i.e., Pd–Cu₂O{100} supported structure) and illustration for the charge transfer on the Cu₂O{100}–Pd interface; (d) photocatalytic hydrogen production from pure water using Cu₂O based catalysts (adapted with permission from ref. 28, Copyright 2014 Wiley-VCH Verlag GmbH & Co.).

interfaces in supported structure and core–shell structure with Pd and Cu₂O as components I and II, respectively.⁴⁰ The Cu₂O nanocrystals in both samples are in a cubic profile with exposed {100} facets to guarantee the Schottky junction formation for hole migration from Cu₂O to Pd. For the Pd–Cu₂O supported structure, a large amount of interfacial defects formed due to the fact that the polycrystalline interface appears as charge recombination centers and disfavors the hole transfer across the interface (Fig. 6a). In comparison, the Pd–Cu₂O core–shell structure possesses a Cu₂O(100)–Pd(100) interface built based on single-crystal cores (Pd cubes) and shells, substantially reducing the number of interfacial defects. However, the intrinsic drawback of this core–shell structure is that the holes trapped in the cores can hardly be delivered beyond the shells for surface reactions (Fig. 6b). To circumvent this undesirable situation, a novel semiconductor–metal–graphene stack structure has been designed by our research group. The stack structure is fabricated by firstly growing {100}-faceted Pd nanocubes on rGO nanosheets and then selectively coating single-crystal Cu₂O shells on the Pd surface (Fig. 6c–e). This ternary structure not only inherits the advantage of core–shell structure in defect elimination, but also offers a new Pd–graphene interface for the holes to migrate out for surface reactions owing to the high charge mobility of graphene (Fig. 6f).⁶¹ First-principles simulations have confirmed that the strong electronic couplings of the Cu₂O–Pd and Pd–rGO interfaces favor smooth charge transfer. As a result, the stack structure shows a significantly higher photocatalytic H₂ production rate in comparison with other Cu₂O based catalysts (Fig. 6g). Moreover, the performance of the stack structure is also superior to the Cu₂O–rGO structures with or without Pd nanoparticles supported on Cu₂O, as the direct Cu₂O–rGO interface is of weak electronic coupling. This finding demonstrates that rational interface design guarantees the high catalytic performance, which cannot be achieved by simply mixing the components. It is worth pointing out that the morphology and composition of stack structures can be well maintained after photocatalysis, further confirming the strong interfacial contact between the components.

It is worth pointing out that in terms of semiconductor–metal interfaces, charge transfer between the semiconductor and the metal by the Schottky junction effect is not the only working mechanism. Some noble metals such as Ag and Au have surface plasmonic properties that may have interactions with the semiconductor through several different mechanisms including: (1) injection of hot carriers into the conduction or valence band of the semiconductor through so-called “direct electron transfer”, (2) local electromagnetic field enhancement mediated by surface plasmon to facilitate the formation of charge carriers in the semiconductor, and (3) energy transfer from localized plasmonic dipoles to electron–hole pairs in semiconductors through resonant energy transfer.^{19,62,63} When the surface plasmon of the metal in a hybrid structure is light excited synchronously, the energy levels of hot carriers are high enough to overcome the Schottky barrier and be injected into the semiconductor. This carrier injection follows an opposite direction to the charge transfer driven by the Schottky junction

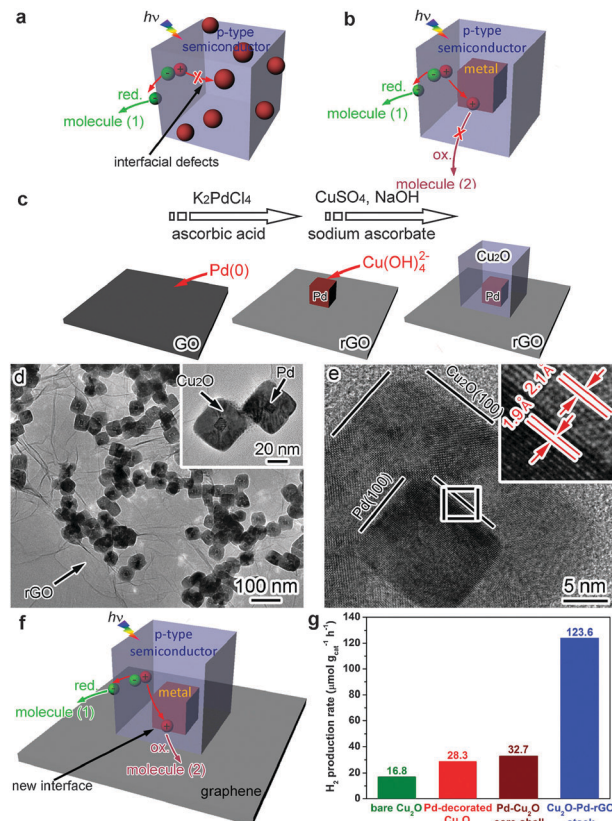


Fig. 6 (a and b) Schematic illustration for the limitation in metal–semiconductor supported structure and core–shell structure for interfacial charge transfer with Pd and Cu₂O as components; (c–e) schematic illustration for the (c) synthetic approach; (d) TEM and (e) HRTEM images of the Cu₂O–Pd–rGO stack structures; (f) schematic illustration for the charge flow in semiconductor–metal–graphene stack design; (g) photocatalytic average rates of hydrogen production under irradiation (adapted with permission from ref. 40, Copyright 2014 Wiley-VCH Verlag GmbH & Co.).

across the same interface, and constitutes a severe competition with the Schottky junction, dramatically reducing the efficiency of charge spatial separation.^{27,64}

This contradiction forces us to perform new interface design when plasmonic metals are excited in the semiconductor–metal junction. An approach to circumvent this undesired situation is to form two different metal–semiconductor interfaces based on the selection of semiconductor facets and metals for the plasmonic effect and the Schottky junction, respectively. Most recently we reported a case of Ag–(001)BiOCl(110)–Pd hybrid structure toward this direction.⁶⁵ The design begins with the facet-dependent charge behavior in UV light-excited p-type BiOCl nanoplates, in which photo-generated holes and electrons are preferentially accumulated on (110) and (001) facets, respectively. Then the interface design is based on the facet-dependent charge accumulation: the first interface is formed between BiOCl(110) and nonplasmonic Pd to establish the Schottky barrier so that the holes can be trapped by the Pd nanocrystals, while the second one is to place visible light-excited plasmonic Ag nanocrystals on BiOCl(001) where the surface plasmon of Ag injects hot holes into BiOCl under visible

illumination. To confirm the rationality of the design, we have investigated the charge behavior from two different angles. On one hand, Pd nanocubes are selectively deposited on different facets of BiOCl to form BiOCl(001)-Pd and BiOCl(110)-Pd hybrid structures, respectively (Fig. 7a–c). From the photocurrents and photocatalytic O₂ evolution under UV light irradiation, it can be recognized that the BiOCl(110)-Pd interface offers prominent hole transfer for reducing the charge recombination in comparison with the BiOCl(001)-Pd interface, showing that the BiOCl(110)-Pd interface should be selected for the Schottky junction (Fig. 7d and e). On the other hand, Ag nanocubes are firstly deposited on BiOCl(001) to obtain the Ag-(001)BiOCl structure, followed by the assembly of Pd nanocubes on the BiOCl(110) facet to produce the designed Ag-(001)BiOCl(110)-Pd structure (Fig. 7f–h). The gradually enhanced photocurrent and photocatalytic O₂ evolution from BiOCl to Ag-BiOCl and then to Ag-BiOCl-Pd structure under visible light irradiation (Fig. 7i and j) verifies that the plasmonic hot holes can be injected from Ag into BiOCl and then be trapped by Pd. As such, the two well-designed interfaces in the Ag-BiOCl-Pd structure offer an ideal platform for integrating the plasmonic effect with the Schottky junction for full-spectrum photocatalysis. As shown in Fig. 7k and l, the photocurrents and

photocatalytic O₂ evolution of the ternary hybrid structure are dramatically larger than those of its component structures. In this ternary structure, the two interfaces steer the charge flow in the Ag-(001)BiOCl(110)-Pd structure by three effects – the Schottky barrier with Pd to extract holes from BiOCl through the BiOCl(110)-Pd interface, and plasmonic deep hole injection from Ag through the Ag-(001)BiOCl interface, together with the intrinsic facet-dependent spatial charge separation in the inner BiOCl (Fig. 7m). In the meantime, the local electromagnetic field of plasmonic Ag also enhances the charge generation in BiOCl.

Co-effects in surface and interface design for catalytic hybrid structures

Based on the individual surface and interface designs discussed above, the designs can be also synergized together to implement their co-effects in photocatalytic and electrocatalytic performance enhancement. On one hand, the interface and the surface of components can be simultaneously tailored for better charge transfer and surface reactions. For instance, we have reported a metal-organic framework (MOF)@semiconductor core-shell structure using Cu₃(BTC)₂ (BTC = benzene-1,3,5-tricarboxylate)

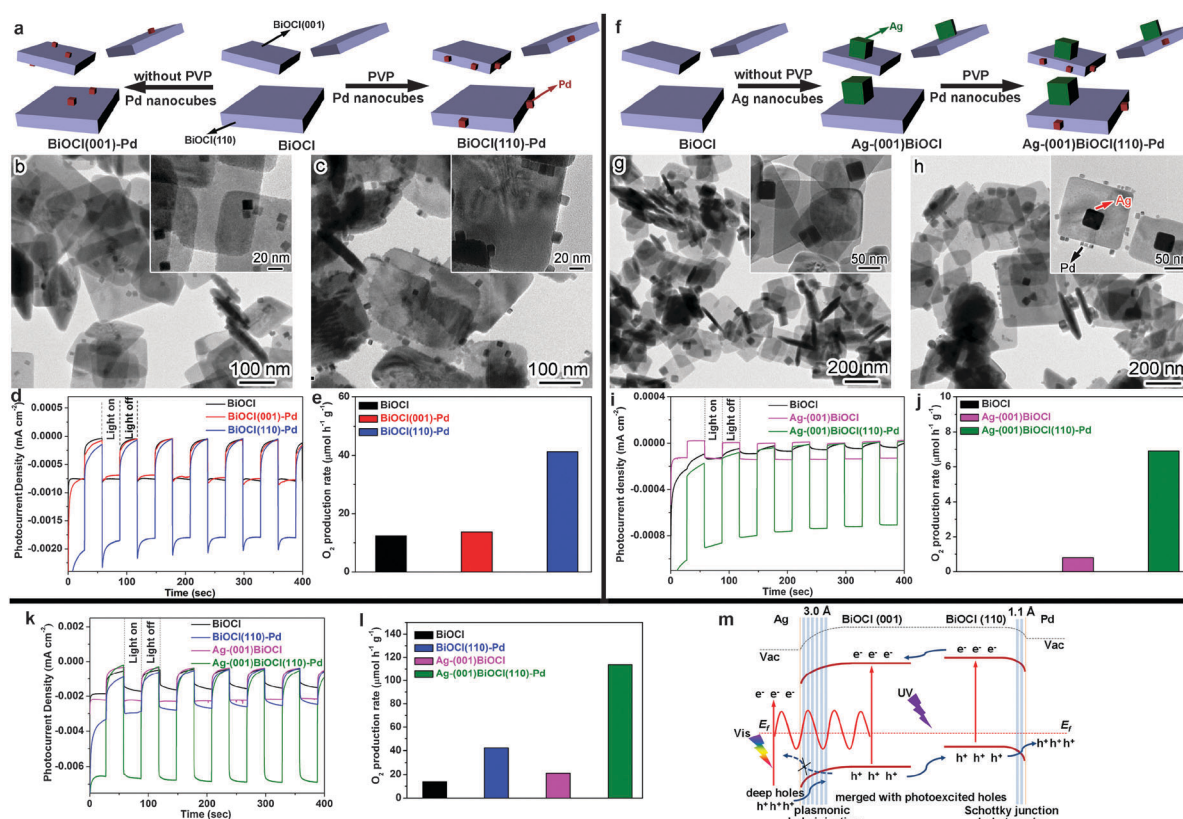


Fig. 7 (a) Schematic illustration for the synthesis of BiOCl-Pd hybrid structures; (b and c) TEM images of BiOCl(001)-Pd and BiOCl(110)-Pd structures; (d and e) photocurrents vs. time (*I*-*t*) curves (d) and photocatalytic O₂ evolution (e) under UV light irradiation; (f) schematic illustration for the synthesis of Ag-BiOCl and Ag-BiOCl-Pd hybrid structures; (g and h) TEM images of Ag-(001)BiOCl and Ag-(001)BiOCl(110)-Pd structures; (i and j) photocurrents vs. time (*I*-*t*) curves (i) and photocatalytic O₂ evolution (j) under visible light irradiation; (k and l) photocurrents vs. time (*I*-*t*) curves (k) and photocatalytic O₂ evolution (l) under full-spectrum irradiation; (m) schematic illustrating the band alignments and charge flow at two metal-semiconductor interfaces in Ag-(001)BiOCl(110)-Pd under full-spectrum irradiation (adapted with permission from ref. 65, Copyright 2015 Wiley-VCH Verlag GmbH & Co.).

and macroporous TiO_2 as components I and II, respectively (Fig. 8a).⁶⁶ In this hybrid structure, the interface between $\text{Cu}_3(\text{BTC})_2$ and TiO_2 not only prolongs the photoexcited carrier lifetime *via* effective electron transfer from TiO_2 to the MOF, but also captures gas molecules and provides reaction sites for CO_2 conversion owing to the unique porous structure of the MOF. As shown in Fig. 8b, both the activity and selectivity in photocatalytic CO_2 reduction have been improved by integrating TiO_2 with the MOF.

On the other hand, some interfacial effects may also alter the electronic state of the surface especially when the interface is sufficiently close to the surface. As such, the ability of the catalyst surface in activating reaction species and participating in reactions would be tuned through a synergistic design of the interface and the surface. A typical case is the surface polarization that we have demonstrated for electrocatalysis most recently. In a hybrid structure, the different work functions of two components may induce polarization at their interface. As long as the distance between the polarized interface and the reactive surface is confined at the atomic level, the charges created by interface polarization can reach the surface, thereby sustaining surface polarization.^{67,68} For instance, the Pt-Pd-rGO stack structures with controllable Pt shell thickness can be obtained by selectively coating Pt on the Pd nanocubes that are supported on rGO nanosheets (Fig. 9a–c).²³ As the obtained Pt-Pd-rGO structures are used as electrocatalysts for hydrogen-evolution reaction (HER), their HER performance can be enhanced with Pt thickness reduction (Fig. 9d and e) with the same Pd and rGO loadings. The mechanism behind is that the work function of the Pt shell is higher than that of the Pd core, which drives the migration of electrons from Pd to Pt so as to equilibrate the electron Fermi distribution at their interface. As proven by first-principles simulations (Fig. 9f), this interfacial polarization increases the electron density of the Pt surface to improve HER activity when the Pt thickness is within a few atomic layers. Apparently, the surface polarization effect would become weaker as the Pt thickness increases. For this reason, less Pt usage leads to better catalytic performance (Fig. 9g). The Pt-Pd interfacial polarization effect, as well as the rGO support facilitating catalyst-electrode electron transfer, contributes to the impressive HER performance of Pt-Pd-rGO I with minimal Pt thickness (Fig. 9d and e).

The interfacial polarization can also be applied to other types of reactions such as CO oxidation. For instance, we have

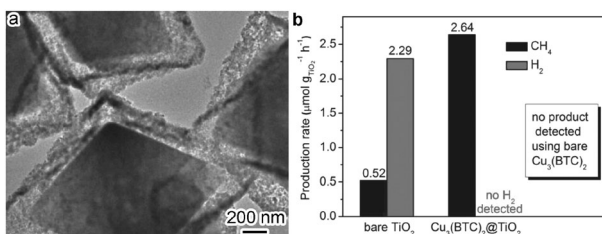


Fig. 8 (a) TEM image of $\text{Cu}_3(\text{BTC})_2@{\text{TiO}_2}$ core–shell structures; (b) production yields of CH_4 and H_2 from CO_2 and H_2O using $\text{Cu}_3(\text{BTC})_2@{\text{TiO}_2}$ core–shell structures in reference to bare TiO_2 nanocrystals (adapted with permission from ref. 66, Copyright 2014 Wiley-VCH Verlag GmbH & Co.).

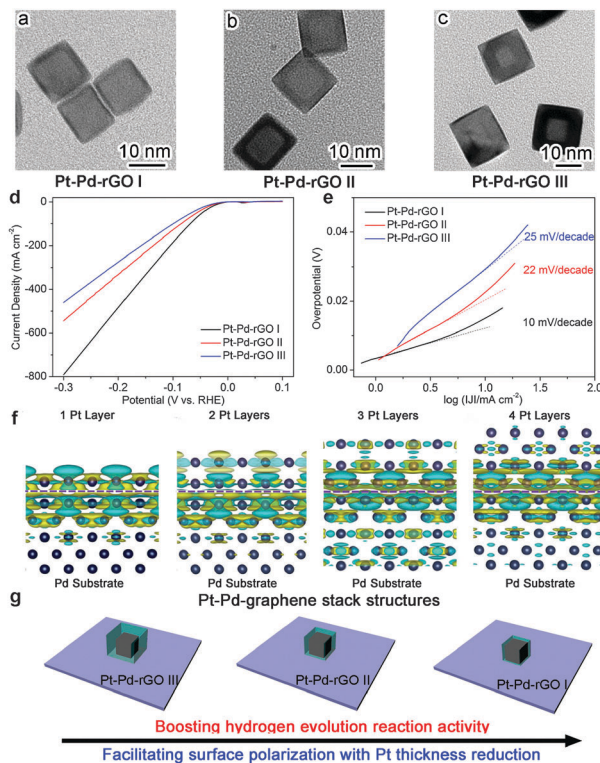


Fig. 9 (a–c) TEM images of (a) Pt-Pd-rGO I, (b) Pt-Pd-rGO II, and (c) Pt-Pd-rGO III with increased Pt thickness; (d) and (e) polarization curves (d) and the corresponding Tafel plots (e) of Pt-Pd-rGO I, II, and III, respectively; (f) differential charge density by first-principles simulations illustrating the alterations of electron distributions with the Pt thickness from 1 to 4 layers on the Pd substrate (olive and cyan represent the increase and decrease in electron density, respectively); (g) schematic illustration for the correlation of HER activity with Pt thickness due to surface polarization (adapted with permission from ref. 23, Copyright 2014 Wiley-VCH Verlag GmbH & Co.).

developed a new class of $\text{Ag}-\text{Cu}_2\text{O}$ hybrid structures where Cu_2O is partially deposited on the area close to the edges of Ag nanoplates, leaving the central part uncovered.¹⁸ Unlike the two-dimensional interface in Pt-Pd-rGO, this one-dimensional interface between metal and oxide is exposed on the surface so that the polarized charges do not need to travel along a long distance. As such, the resulted surface polarization becomes more prominent. By controlling the coverage area of Cu_2O , the lengths of exposed $\text{Ag}-\text{Cu}_2\text{O}$ interfacial lines can be tuned from partial coverage I to III (Fig. 10a–c). When the $\text{Ag}-\text{Cu}_2\text{O}$ structures are used for catalytic CO oxidation, the Cu_2O surface can be oxidized to CuO in the first cycle. Starting from the second cycle, the CO conversion rates turn out to decrease with the reduction of $\text{Ag}-\text{CuO}$ interfacial lengths at all temperatures (Fig. 10d and e), indicating the role of interfacial lines as active sites. Specifically, the work function difference induces the charge flow from Ag (lower work function) to CuO (higher work function). This interfacial polarization makes the CuO surface next to the interfacial lines particularly active for CO oxidation (Fig. 10f). The interfacial polarization has been proven by first-principles simulations, in which a significant increase in electron density has been observed at the CuO surface, along

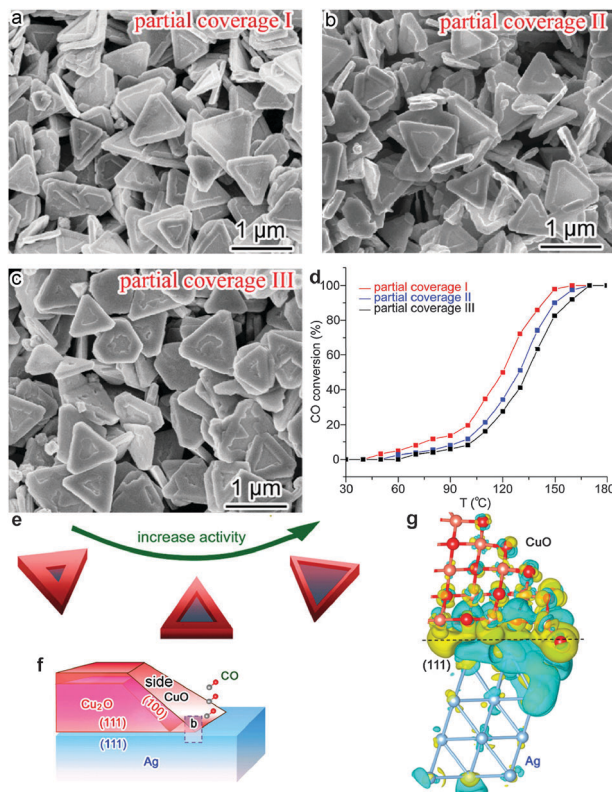


Fig. 10 (a–c) SEM images of Ag–Cu₂O with partial coverage I, II, and III, respectively (*i.e.*, reduced interfacial line lengths); (d) catalytic performance of Ag–CuO/Cu₂O partial coverage I, II and III in cycle 2 of CO oxidation; (e) schematic illustration for the correlation of CO oxidation activity with the Ag–Cu₂O interfacial line length; (f) schematic illustration for Ag–CuO/Cu₂O hybrid structures with interface polarization for CO oxidation (side view for the cross-section); (g) differential charge density by first-principles simulations illustrating the increase (olive color) and decrease (cyan color) of electron distributions in the atomic model for the Ag(111) substrate interfacing with the extension part of the side CuO layer (adapted with permission from ref. 18, Copyright 2014 American Chemical Society).

with the reduction of electron density at the interface layer of Ag(111) (Fig. 10g). As a result, the catalytic activities have a strong correlation with the number of active sites on CuO along the interfacial lines, and thus longer interfacial lines lead to higher catalytic activity.

Summary and outlook

Surface and interface design for catalytic hybrid structures represents an interesting and important development direction toward enhanced performance in various electrocatalytic and photocatalytic reactions. In this Feature Article, we summarize the recent progress reported by our group that tailors the surface and the interface of well-defined catalytic hybrid structures through controlled synthesis, upon elaborating the designing rules. For surface design, the parameters including exposed facets, areas, compositions and phases have been tailored to improve catalytic activity and selectivity in photocatalysis and electrocatalysis. In terms of interface design, the

selection of an appropriate surface to form the interface and the interfacial parameters critical to the electronic contact between two components have shown their importance for facilitating the charge spatial separation in photocatalysis. Meanwhile, the surface and interface design has also been combined toward their co-effects of synergistic interactions. In particular, the surface polarization effect offers an excellent platform for maneuvering surface activity through forming a well-designed interface, which can be extended to other reaction types.

Despite the success by our research group and many other researchers, the research on surface and interface design for catalytic hybrid structures still has a long way to go. Both challenges and opportunities are awaiting the research of fabricating novel hybrid catalytic systems in terms of surface and interface engineering. One of the challenges is that synthesis techniques have lagged behind our demands to realize theoretical designs by precisely controlling parameters. From the viewpoint of mechanism studies, thus far characterization techniques can barely give a clear picture on the variations in some parameters such as surface vacancies and interface defects. This limitation of characterization makes many deep mechanisms behind structure–property relationships remain elusive, formulating an obstacle to further optimize materials design. The existing theories and models have been proposed mainly based on the collected experimental data together with theoretical simulations, whose precision may be limited by the resolutions of characterization and simulations. As more components are involved in the design of hybrid structures, working mechanisms would undoubtedly become more complicated. Thus *in situ* observation and detection techniques at high spatial, spectral and temporal resolutions are highly desirable for enabling deeper understanding. All in all, the invention or upgradation of various new techniques is anticipated to bring about many exciting research opportunities to the development of surface and interface design for catalytic hybrid structures in the future.

Acknowledgements

This work was financially supported by 973 Program (No. 2014CB848900), NSFC (No. 21471141, 21101145, and 91123010), Recruitment Program of Global Experts, CAS Hundred Talent Program, and Fundamental Research Funds for the Central Universities (No. WK2060190025 and WK2310000035).

Notes and references

- J. A. Schwarz, C. Contescu and A. Contescu, *Chem. Rev.*, 1995, **95**, 477.
- J. K. Nørskov, T. Bligaard, J. Rossmeisl and C. H. Christensen, *Nat. Chem.*, 2009, **1**, 37.
- G. Liu, H. G. Yang, J. Pan, Y. Q. Yang, G. Q. Lu and H. M. Cheng, *Chem. Rev.*, 2014, **114**, 9559.
- J. Gong, *Chem. Rev.*, 2012, **112**, 2987.
- H. Zhang, M. Jin, Y. Xiong, B. Lim and Y. Xia, *Acc. Chem. Res.*, 2013, **46**, 1783.

- 6 H. Tong, S. Ouyang, Y. Bi, N. Umezawa, M. Oshikiri and J. Ye, *Adv. Mater.*, 2012, **24**, 229.
- 7 S. Guo, S. Zhang and S. Sun, *Angew. Chem., Int. Ed.*, 2013, **52**, 8526.
- 8 R. Bashyam and P. Zelenay, *Nature*, 2006, **443**, 63.
- 9 J. Shi, *Chem. Rev.*, 2013, **113**, 2139.
- 10 Q. Xiang, J. Yu and M. Jaroniec, *Chem. Soc. Rev.*, 2012, **41**, 782.
- 11 G. Xie, K. Zhang, B. Guo, Q. Liu, L. Fang and J. R. Gong, *Adv. Mater.*, 2013, **25**, 3820.
- 12 M. Liu, R. Zhang and W. Chen, *Chem. Rev.*, 2014, **114**, 5117.
- 13 K. I. Hadjiiivanov and D. G. Klissurski, *Chem. Soc. Rev.*, 1996, **25**, 61.
- 14 F. Tao, *Chem. Soc. Rev.*, 2012, **41**, 7977.
- 15 Z. C. Zhang, B. Xu and X. Wang, *Chem. Soc. Rev.*, 2014, **43**, 7870.
- 16 Y. Ma, X. Wang, Y. Jia, X. Chen, H. Han and C. Li, *Chem. Rev.*, 2014, **114**, 9987.
- 17 Y. Zhang, N. Zhang, Z. R. Tang and Y. J. Xu, *Phys. Chem. Chem. Phys.*, 2012, **14**, 9167.
- 18 Y. Bai, W. Zhang, Z. Zhang, J. Zhou, X. Wang, C. Wang, W. Huang, J. Jiang and Y. Xiong, *J. Am. Chem. Soc.*, 2014, **136**, 14650.
- 19 S. Bai, J. Jiang, Q. Zhang and Y. Xiong, *Chem. Soc. Rev.*, 2015, **44**, 2893.
- 20 R. Long, S. Zhou, B. J. Wiley and Y. Xiong, *Chem. Soc. Rev.*, 2014, **43**, 6288.
- 21 Y. Xia, Y. Xiong, B. Lim and S. E. Skrabalak, *Angew. Chem., Int. Ed.*, 2009, **48**, 60.
- 22 L. Ma, C. Wang, B. Y. Xia, K. Mao, J. He, X. Wu, Y. Xiong and X. W. Lou, *Angew. Chem., Int. Ed.*, 2015, **54**, 5666.
- 23 S. Bai, C. Wang, M. Deng, M. Gong, Y. Bai, J. Jiang and Y. Xiong, *Angew. Chem., Int. Ed.*, 2014, **53**, 12120.
- 24 D. Liu, L. Li, Y. Gao, C. Wang, J. Jiang and Y. Xiong, *Angew. Chem., Int. Ed.*, 2015, **54**, 2980.
- 25 R. Long, K. Mao, X. Ye, W. Yan, Y. Huang, J. Wang, Y. Fu, X. Wang, X. Wu, Y. Xie and Y. Xiong, *J. Am. Chem. Soc.*, 2013, **135**, 3200.
- 26 R. Long, Z. Rao, K. Mao, Y. Li, C. Zhang, Q. Liu, C. Wang, Z. Y. Li, X. Wu and Y. Xiong, *Angew. Chem., Int. Ed.*, 2015, **54**, 2425.
- 27 R. Long, K. Mao, M. Gong, S. Zhou, J. Hu, M. Zhi, Y. You, S. Bai, J. Jiang, Q. Zhang, X. Wu and Y. Xiong, *Angew. Chem., Int. Ed.*, 2014, **53**, 3205.
- 28 L. Wang, J. Ge, A. Wang, M. Deng, X. Wang, S. Bai, R. Li, J. Jiang, Q. Zhang, Y. Luo and Y. Xiong, *Angew. Chem., Int. Ed.*, 2014, **53**, 5107.
- 29 C. Wang, L. Ma, L. Liao, S. Bai, R. Long, M. Zuo and Y. Xiong, *Sci. Rep.*, 2013, **3**, 2580.
- 30 Z. W. Seh, S. Liu, M. Low, S. Y. Zhang, Z. Liu, A. Mlayah and M. Y. Han, *Adv. Mater.*, 2010, **24**, 2310.
- 31 M. Shim, H. McDaniel and N. Oh, *J. Phys. Chem. Lett.*, 2011, **2**, 2722.
- 32 G. Zhu and Z. Xu, *J. Am. Chem. Soc.*, 2011, **133**, 148.
- 33 Z. Li, C. Li, Y. Mei, L. Wang, G. Du and Y. Xiong, *Nanoscale*, 2013, **5**, 3030.
- 34 J. Li, S. K. Cushing, J. Bright, F. Meng, T. R. Senty, P. Zheng, A. D. Bristow and N. Wu, *ACS Catal.*, 2013, **3**, 47.
- 35 C. H. Kuo, T. E. Hua and M. H. Huang, *J. Am. Chem. Soc.*, 2009, **133**, 17871.
- 36 H. Sun, J. He, J. Wang, S. Y. Zhang, C. Liu, T. Sritharan, S. Mhaisalkar, M. Y. Han, D. Wang and H. Chen, *J. Am. Chem. Soc.*, 2013, **135**, 9099.
- 37 S. Bai, X. Shen, G. Zhu, M. Li, H. Xi and K. Chen, *ACS Appl. Mater. Interfaces*, 2012, **4**, 2378.
- 38 C. Song, J. M. Garce and Y. Sugi, *Shape-selective catalysis*, ACS Symposium Series eBooks, 2000.
- 39 M. Kong, Y. Li, X. Chen, T. Tian, P. Fang, F. Zheng and X. Zhao, *J. Am. Chem. Soc.*, 2011, **133**, 16414.
- 40 S. Bai, J. Ge, L. Wang, M. Gong, M. Deng, Q. Kong, L. Song, J. Jiang, Q. Zhang, Y. Luo, Y. Xie and Y. Xiong, *Adv. Mater.*, 2014, **26**, 5689.
- 41 L. Ma, C. Wang, M. Gong, L. Liao, R. Long, J. Wang, D. Wu, W. Zhong, M. J. Kim, Y. Chen, Y. Xie and Y. Xiong, *ACS Nano*, 2012, **6**, 9797.
- 42 S. Bai and Y. Xiong, *Sci. Adv. Mater.*, DOI: 10.1166/sam.2015.2261.
- 43 S. Bai and X. Shen, *RSC Adv.*, 2012, **2**, 64.
- 44 S. Bai, C. Wang, W. Jiang, N. Du, J. Li, J. Du, R. Long, Z. Li and Y. Xiong, *Nano Res.*, DOI: 10.1007/s12274-015-0770-6.
- 45 Y. Bai, R. Long, C. Wang, M. Gong, Y. Li, H. Huang, H. Xu, Z. Li, M. Deng and Y. Xiong, *J. Mater. Chem. A*, 2013, **1**, 4228.
- 46 Y. Bi, S. Ouyang, N. Umezawa, J. Cao and J. Ye, *J. Am. Chem. Soc.*, 2011, **133**, 6490.
- 47 L. Liu, H. Zhao, J. M. Andino and Y. Li, *ACS Catal.*, 2012, **2**, 1817.
- 48 M. Guan, C. Xiao, J. Zhang, S. Fan, R. An, Q. Cheng, J. Xie, M. Zhou, B. Ye and Y. Xie, *J. Am. Chem. Soc.*, 2013, **135**, 10411.
- 49 H. Xu, P. Reunchan, S. Ouyang, H. Tong, N. Umezawa, T. Kako and J. Ye, *Chem. Mater.*, 2013, **25**, 405.
- 50 J. Yang, D. Wang, H. Han and C. Li, *Acc. Chem. Res.*, 2013, **46**, 1900.
- 51 S. Bai, X. Wang, C. Hu, M. Xie, J. Jiang and Y. Xiong, *Chem. Commun.*, 2014, **50**, 6094.
- 52 S. Bai, L. Wang, X. Chen, J. Du and Y. Xiong, *Nano Res.*, 2015, **8**, 175.
- 53 T. F. Jarlamillo, K. P. Jorgensen, J. Bonde, J. H. Nielsen, S. Horch and I. Chorkendorff, *Science*, 2007, **317**, 100.
- 54 F. K. Meng, J. T. Li, S. K. Cushing, M. J. Zhi and N. Q. Wu, *J. Am. Chem. Soc.*, 2013, **135**, 10286.
- 55 M. A. Lukowski, A. S. Daniel, F. Meng, A. Forticaux, L. S. Li and S. Jin, *J. Am. Chem. Soc.*, 2013, **135**, 10247.
- 56 T. Torimoto, H. Horibe, T. Kameyama, K. Okazaki, S. Ikeda, M. Matsumura, A. Ishikawa and H. Ishihara, *J. Phys. Chem. Lett.*, 2011, **2**, 2057.
- 57 P. Zhou, J. Yu and M. Jaroniec, *Adv. Mater.*, 2014, **26**, 4920.
- 58 A. L. Linsebigler, G. Lu and J. T. Yates Jr., *Chem. Rev.*, 1995, **95**, 735.
- 59 W. Fan, Q. Zhang and Y. Wang, *Phys. Chem. Chem. Phys.*, 2013, **15**, 2632.
- 60 R. Li, F. Zhang, D. Wang, J. Yang, M. Li, J. Zhu, X. Zhou, H. Fan and C. Li, *Nat. Commun.*, 2013, **4**, 1432.
- 61 S. Bai, X. Shen, H. Lv, G. Zhu, C. Bao and Y. Shan, *J. Colloid Interface Sci.*, 2013, **405**, 1.
- 62 S. Linic, P. Christopher and D. B. Ingram, *Nat. Mater.*, 2011, **10**, 911.
- 63 S. K. Cushing, J. Li, F. Meng, T. R. Senty, S. Suri, M. Zhi, M. Li, A. D. Bristow and N. Wu, *J. Am. Chem. Soc.*, 2012, **134**, 15033.
- 64 C. G. Silva, R. Juárez, T. Marino, R. Molinari and H. García, *J. Am. Chem. Soc.*, 2011, **133**, 595.
- 65 S. Bai, X. Li, Q. Kong, R. Long, C. Wang, J. Jiang and Y. Xiong, *Adv. Mater.*, DOI: 10.1002/adma.201501200.
- 66 R. Li, J. Hu, M. Deng, H. Wang, X. Wang, Y. Hu, H. L. Jiang, J. Jiang, Q. Zhang, Y. Xie and Y. Xiong, *Adv. Mater.*, 2014, **26**, 4783.
- 67 C. G. Vayenas, S. Bebelis and S. Ladas, *Nature*, 1990, **343**, 625.
- 68 Y. N. Sun, L. Giordano, J. Goniakowski, M. Lewandowski, Z. H. Qin, C. Noguera, S. Shaikhutdinov, G. Pacchioni and H. J. Freund, *Angew. Chem., Int. Ed.*, 2010, **49**, 4418.